2016-01-0159
Published 04/05/2016

doi:10.4271/2016-01-0159
saepcelec.saejournals.org

Grid-Tied Single-Phase Bi-Directional PEV Charging/Discharging Control

Luting Wang, Chong Cao, and Bo Chen
Michigan Technological Univ

ABSTRACT

This paper studies the bi-directional power flow control between Plug-in Electric Vehicles (PEVs) and an electrical grid. A grid-tied charging system that enables both Grid-to-Vehicle (G2V) and Vehicle-to-Grid (V2G) charging/discharging is modeled using SimPowerSystems in Matlab/Simulink environment. A bi-directional AC-DC converter and a bi-directional DC-DC buck-boost converter are integrated to charge and discharge PEV batteries. For AC-DC converter control, Predictive Current Control (PCC) strategy is employed to enable grid current to reach a reference current after one modulation period. In addition, Phase Lock Loop (PLL) and a band-stop filter are designed to lock the grid voltage phase and reduce harmonics. Bi-directional power flow is realized by controlling the mode of the DC-DC converter. Simulation tests are conducted to evaluate the performance of this bi-directional charging system. The simulation results show that the integrated PCC, PLL, and band-stop filter can achieve fast dynamic response, low Total Harmonics Distortion (THD) of grid voltage and current, and unity power factor.

Keywords: Plug-in Electric Vehicles, bi-directional power flow, PWM AC-DC converter, PWM DC-DC buck-boost converter, Vehicle to Grid, Predictive Current Control, Phase Lock Loop, band-stop filter, Total Harmonic Distortion, unity power factor

CITATION: Wang, L., Cao, C., and Chen, B., "Grid-Tied Single-Phase Bi-Directional PEV Charging/Discharging Control," *SAE Int. J. Passeng. Cars – Electron. Electr. Syst.* 9(2):2016, doi:10.4271/2016-01-0159.

INTRODUCTION

PEVs are being increasingly adopted in transportation systems as environmentally friendly vehicles. U.S. Environmental Protection Agency (EPA) and the National Highway Traffic Safety Administration (NHTSA) have jointly developed a fuel economy & greenhouse gas standard to regulate the greenhouse gas emission and fuel economy [1]. According to Vehicle Technology Office of the Department of Energy (DOE), transitioning to a light-duty fleet Hybrid Electric Vehicles (HEVs) and PEVs could reduce U.S. foreign oil dependence by 30-60% and greenhouse gas emissions by 30-45% [2]. As the fast development of PEVs and their deep penetration into distribution system, the interaction between PEVs and grid becomes a new challenge. The need to charge large amount of PEVs bring a heavy burden on existing electricity grid. In addition, there are some scenarios where vehicles are required to operate in reverse power flow mode, Vehicle-to-Grid (V2G) mode in which PEVs behave as an electrical energy resource to offer power support and balancing. From this perspective, the bi-directional power flow technology plays a crucial role between PEVs and grid. To realize the bi-directional energy flow between the grid and PEVs, a number of research work has been conducted and reported, which is summarized in three aspects.

The first aspect is the study of rectifier/inverter control strategies. For single phase AC-DC converters, the control strategies can be classified as indirect current control and direct current control. Indirect current control is a phasor control method that indirectly control the grid-side line current based on its relation with grid-side voltage. This method can achieve good transient performance, however, the current response is slow [3, 4]. Direct current control method directly controls the sensed grid-side current that gets faster current response. Direct current control is the major control method researchers used, such as the ramp comparison, hysteresis control, predictive current control, and Delta modulation controls [5, 6]. Ramp comparison is a conventional control method, by which a tri-angular waves is used to compare with the line current error to generate PWM signals. However, the crossing effect that results from phase and amplitude errors of line current [5] or improperly selected carrier frequency [7] is unneglectable. Hysteresis control utilizes hysteresis comparator to restrict the error between sensed current and reference current and generate PWM signals accordingly. Hysteresis controllers have the advantages of fast dynamic response, fine robustness, simple structure, and easy to achieve, but also have undesirable current harmonics ripple due to variable switching frequency that highly depends on load parameters [8, 10]. Predictive current control forces the grid-side current to track a reference current in one switching period, and the DC-link voltage is used to estimate the reference current for the sensed line current. This method has a fixed frequency and the best potential to achieve good current regulation with less distortion and harmonics [8, 9, 10,]. However, the robustness is poor and the transient overshoot is higher than hysteresis control method, hence, a good knowledge of the system is required [6, 10, 11, 12]. In this paper, one goal is to achieve low current harmonics, as a tradeoff, those disadvantages are minimized, and the predictive current control method is selected.

The second aspect is the control strategies for bi-directional DC-DC converters. Prior research work for the application in electric vehicles includes the bi-directional power flow between batteries and motors [13, 14] and energy transfer between the battery and high-voltage bus [15]. Most existing literature studies the control methods based on resistive load. In addition, the control strategies mainly focus on generating a constant DC-link voltage to feed passive loads instead of providing a reasonable charging method, like, constant current (CC) or constant voltage (CV). Therefore, these control methods may not applicable for G2V or V2G applications.

The last but most important aspect is the integration of bi-directional charging system and PEVs' batteries with the grid. As aforementioned, a lot of work have been done at component level of the charging system. Further study is needed at system level to ensure the performance of an integrated system. In existing literature, charger research mainly focuses on three-phase converter control and the power flow is mostly unidirectional [16,17,18]. In [18], AC Voltage Sensorless control is studied for the control of a bridgeless power factor correction AC-DC converter. A DC-DC buck converter is utilized to charge the battery. This charging system has high power factor but can't realize bidirectional power flow [18, 19]. In Berker's paper [20], a simplified control strategy is designed to eliminate controller parameters setting. The controlled output has fast enough transients, but the ripples in both current and voltage are higher compared with conventional PI controller due to sampling-time-dependent switching frequency. Some other work uses power control method to realize bi-directional power flow capability [21, 22], but lacks of battery voltage and current analysis. Another research work [23] applies load frequency control strategy to achieve bi-directional power flow, however, the odd order current distortion is not considered. For the voltage and current control, conventional inner-current loop and outer-voltage loop controlled PWM converters are adopted in [16, 22, 24, 25, 26]. Encouragingly, in [27], a set of experimental results are completed with predictive current control method, this provides a good reference for the model-based study in this paper.

In this paper, a bi-directional charger is designed for the following objectives: enabling bi-directional power flow; meeting the harmonic limits requirement of THD defined in IEEE Std 519-1992 [28], and having unity power factor. The rest of the paper is organized as follows. In section 2, the configuration of the charging system is demonstrated. In section 3, a 240 VAC single split phase power source is simulated. In section 4, the battery selection and major battery parameters are discussed, meanwhile SAE standardized charging levels are briefly introduced as well. In section 5, the bi-directional AC-DC converter model and control strategy are introduced, respectively. In section 6, the working principle and control strategy of bi-directional DC-DC converter are illustrated. In section 7, simulation results are presented and analyzed. Finally, the conclusions are made in section 8.

THE CONFIGURATION OF GRID CONNECTED BIDIRECTIONAL PEV CHARGING SYSTEM

Figure 1 shows an overview of the presented bi-directional PEV charging system. The charging system consists of three parts, power grid, charger module, and battery pack. A phase-split transformer is used to generate 240V AC source. In G2V mode, the AC-DC converter behaves as a rectifier to convert sinusoidal voltage to a desired constant DC voltage and the DC-DC converter works in buck mode to charge the battery. In V2G mode, AC-DC converter performs as an inverter and DC-DC converter works in boost mode to feed the energy stored in battery to the grid. PCC strategy is employed to generate PWM signals for AC-DC converter. PLL technique is applied to adjust the grid voltage phase error due to the discrete sampling and control delay. A band-stop filter is used to get rid of odd order harmful harmonics pollution in reference AC current. Constant current - constant voltage (CC-CV) control strategy is used to achieve desired direction of power flow. The design and control of individual components are presented in the following sections.

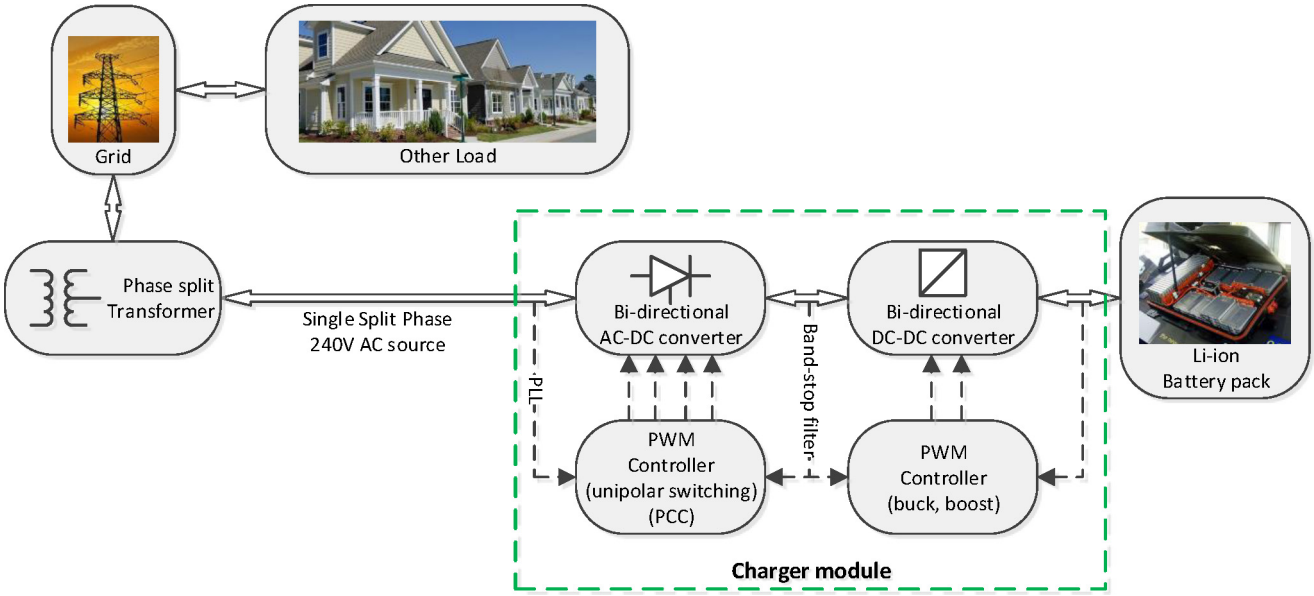

Figure 1. Overview of the presented Bi-directional PEV charging/discharging system

240 VAC SINGLE SPLIT PHASE POWER SOURCE

Figure 2 shows the Simulink model of single split phase, three wires distribution system. In North American distribution system, residential area receives power from 120V/240V split phase source that is fed from a phase split transformer. According to the standard of the distribution system, the primary side of the transformer can be 2.4kV, 7.2kV, 12.47kV, 13.2kV, or 13.8kV. In this paper, a three phase voltage source with 13.2kV of phase-to-phase voltage is selected as the grid source.

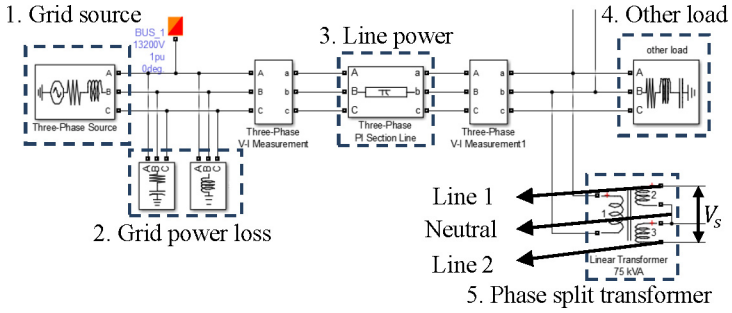

Figure 2. Simulink model of 240 VAC Single Split phase source

In Figure 2, block 1 is the 13.2kV grid source. Block 2 simulates the power loss between grid source and the first node. Block 3 is a Three-Phase PI Section Line that implements a balanced three-phase transmission line model where the resistance, inductance, and capacitance are uniformly distributed along the line in a PI section. Block 4 represents other loads connected to the grid. In real world, the power loss in transmission and distribution networks highly depends on the physical characteristics of the system, and a loss around 7% is typical [29]. The primary side of the split phase transformer is connected to any two of the three phases that has a phase-to-phase voltage of 13.2kV. The secondary side of the transformer has a grounded center tap that supplies two 120 VAC voltage V_{L1N} and V_{L2N} from Line 1 and Line 2. The voltage V_{12} between Line1 and Line 2 is 240 VAC.

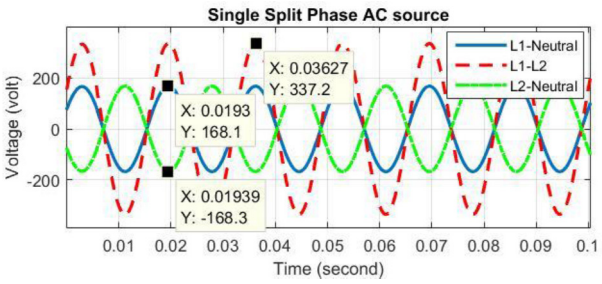

Figure 3. Single Split phase voltage waveforms

In Figure 3, it is observed that V_{L1N} and V_{L2N} have 180 degrees phase difference, and V_{12} has the same phase as V_{L1N} . According to equations (1) and (2), the peak value of each waveform shown in Figure 3 proves the validity of split phase model design.

$$V_{L1N_{peak}} = V_{L2N_{peak}} = 120V \times \sqrt{2} = 169.7V \quad (1)$$

$$V_{12_{peak}} = 240V \times \sqrt{2} = 339.4V \quad (2)$$

PEV BATTERY CHARACTERISTICS

Battery Selection

The main types of battery used in PEVs are NiMH and Li-ion batteries. Due to higher energy capacity and longer lifetime, Li-ion batteries are preferred in PEV applications even though the price is higher. In this paper, the main parameters of the battery cell and battery module use the parameters of Nissan Leaf battery [30]. The specifications of the simulated battery are listed in Table 1.

Table 1. Battery Specifications

Pack Specification	
Nominal voltage	180 V
Number of modules in a pack	24
Module Specification	
Number of cells in a module	4 (prismatic cells)
Construction	2 in-series pairs in parallel
Cell Specification	
Rated capacity	33.1 Ah (0.3C)
Nominal (Average) voltage	3.8 V

The battery model in SimPowerSystems is a generic dynamic model as shown in Figure 4 [31, 32]. The battery current is positive at discharging and negative at charging. The relation between v_{batt} and E_{batt} is shown in equation (3).

$$v_{batt} = E_{batt} - i_{batt} \times R_{int} \quad (3)$$

where, E_{batt} is a nonlinear voltage source (V); v_{batt} is the terminal voltage; R_{int} is the internal resistance; and i_{batt} is Battery current (A).

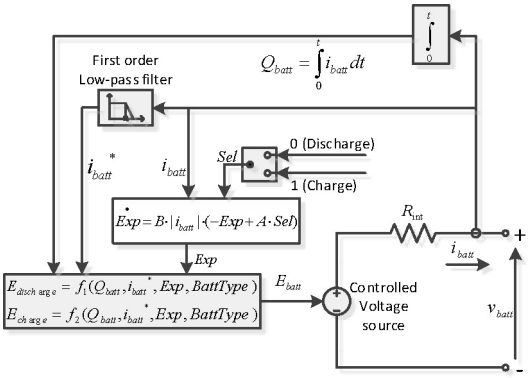

Figure 4. Battery model in SimPowerSystems

The battery type is Lithium-ion. The charge and discharge voltage source is calculated by equation (4) [32].

$$\begin{cases} E_{batt} = E_{discharge} = f_1(Q_{batt}, i^*_{batt}, Exp, BattType) \\ = E_0 - K \cdot \frac{Q}{Q - Q_{batt}} \cdot i^*_{batt} - K \cdot \frac{Q}{Q - Q_{batt}} \cdot Q_{batt} + A \cdot \exp(-B \cdot Q_{batt}) \\ (i^*_{batt} > 0) \\ E_{batt} = E_{charge} = f_2(Q_{batt}, i^*_{batt}, Exp, BattType) \\ = E_0 - K \cdot \frac{Q}{Q_{batt} + 0.1 \cdot Q} \cdot i^*_{batt} - K \cdot \frac{Q}{Q - Q_{batt}} \cdot Q_{batt} + A \cdot \exp(-B \cdot Q_{batt}) \\ (i^*_{batt} < 0) \end{cases} \quad (4)$$

where, E_0 is the battery constant voltage (V); *Exp* represents exponential zone voltage (V); *Sel* represents the battery mode, 0 means charging, 1 means discharging; K is the polarization constant (Ah^{-1}); i^*_{batt} is the low frequency current component (A); Q is the maximum battery capacity (Ah); A is the initial voltage of exponential zone (V); and B is the exponential capacity ($(Ah)^{-1}$).

Two battery parameters, the nominal voltage and rated capacity, are obtained from table 1, and the other parameters use the default setting of battery block based on battery type and nominal values. The nominal current discharge characteristics of battery are shown in Figure 5. The higher current results in faster discharge.

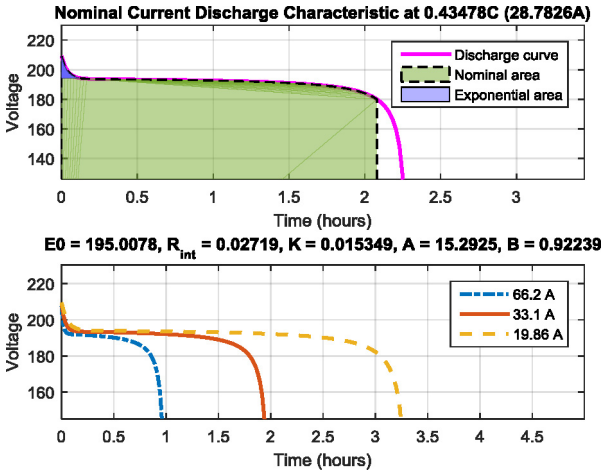

Figure 5. Battery Discharge Characteristic Curve.

PEV Charging Level

In Table 2, the charging levels defined by SAE J1772 standard [33] are summarized. In this paper, the model is built for AC Level 2. The charger power of AC Level 2 can be up to 19.2 kW and the charging current varies from 19.2A to 80A. To test the charger performance at high power, 80 amp charging condition is simulated.

Table 2. Summary of PEV Charging Levels

Charging Level	Power Supply	Charger Power	Miles Range for 1 hour charge	Charge Time (empty to full)
AC Level 1	120VAC Single phase	1.4 kW @12 amp, 1.92kW @16amp (on-board)	~3-5 miles	~17 hours
AC Level 2	208-240VAC Single phase up to 19.2 kW (up to 80 amps)	3.3 kW (on-board)	~8-10 miles	~7 hours
		6.6 kW (on-board)	~17-20 miles	~3.5 hours
DC Level 1	200-450 VDC (up to 80 amps)	19.2kW (residential) & 36kW (public)	~50-60 miles	~28-36 minutes
DC Level 2 Fast charging	200-450 VDC Up to 90kW (approximately 200 amp)	45 kW (off-board)	~50-60 miles (~80% per 0.5 hour charge)	~10-13 minutes

BI-DIRECTIONAL PWM AC-DC CONVERTER

Converter Model Structure

The Bi-directional full-bridge PWM AC-DC converter is the interface between the single phase AC grid and the DC-DC converter. The converter model structure is shown in Figure 6.

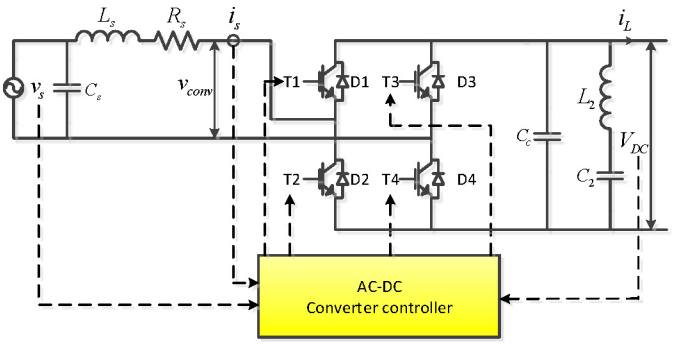

Figure 6. AC-DC converter simulation model

This unipolar PWM converter consists of four IGBT switches with internal antiparallel diodes, two inductors, and three capacitors. The pair of capacitor and inductor on the input side (L_s, C_s) is the AC input filter, and the other pair of capacitor and inductor is the secondary DC output filter (L_2, C_2). C_c is the DC-link capacitor.

The inductor L_s is designed to filter current ripple and the capacitor C_c is used to maintain a constant DC output. In Figure 6, the fundamental component of PWM switch is given by v_{conv}. The value of R_s is small enough to be ignored. According to the circuit, following equations are obtained.

$$v_s = v_{conv} + v_{L_s} \quad (5)$$

$$v_{L_s} = L_s \frac{di_s}{dt} \quad (6)$$

A phasor diagram corresponding to equation (5) is shown in Figure 7 at the frequency of $\omega = 2\pi f$, and $f = 60Hz$.

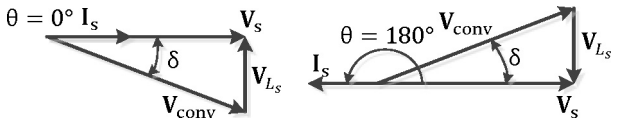

a. b.

Figure 7. AC-DC converter phasor diagram. a. Rectification; b. Inversion

In Figure 7, the relations between each phasor component are given as equations below:

$$\boldsymbol{V}_s = \boldsymbol{V}_{conv} + \boldsymbol{V}_{L_s} \quad (7)$$

$$\boldsymbol{V}_s = V_s e^{j0^\circ} \quad (8)$$

$$\boldsymbol{V}_{L_s} = j\omega L_s \boldsymbol{I}_s \tag{9}$$

So, for both cases, rectification and inversion, the magnitude of each phasor can be obtained, and the inductor value is calculated in equation (10) and (11).

$$V_{conv} = \sqrt{V_s^2 + (\omega L_s I_s)^2} \tag{10}$$

$$L_s = \sqrt{(V_{conv}^2 - V_s^2)/(\omega^2 I_S^2)} \tag{11}$$

The AC side inductor L_s is selected as $2mH$. A 0.003 Ω cascade resistance R_s is added to simulate the line power loss. Assuming no energy stored in the converter, the DC link capacitor is calculated by equating output power to input power without considering switching loss and heat loss.

$$Power_{out} = Power_{in} = 19.2kW \tag{12}$$

$$V_{out} = V_{DC} = 400V \tag{13}$$

$$I_{out} = I_{DC} = \frac{Power_{out}}{V_{out}} = \frac{19.2kW}{400V} = 48A \tag{14}$$

$$X_c = \frac{1}{2\pi f C_c} = \frac{V_{out}}{I_{out}} = \frac{400V}{48A} = 8.33\Omega \tag{15}$$

$$C_c = \frac{1}{2\pi f X_c} = 319.6\mu F \tag{16}$$

The calculated capacitor value is the minimum value, after repeating several simulation testing, it is selected as $8000\mu F$. A secondary LC filter is added paralleled with C_c, the values are selected as $L_2 = 0.84mH$ and $C_2 = 3mF$.

Control Method for AC-DC Converter

The voltage source converter is controlled by Pulse Width Modulation (PWM) switching signals. Four switching signals are needed for a full bridge converter. The conventional dual loop PI control algorithm is shown in Figure 8. The outer voltage control loop generates magnitude reference for inner current control loop by comparing the sensed DC voltage V_{DC} and reference DC voltage V_{DC}^*. The magnitude reference is multiplied with the phase reference provided by the grid voltage v_s. With this configuration, the second order harmonic on DC link voltage introduced by the reference current of the inner current control loop may generate odd harmonics pollution on grid-side current.

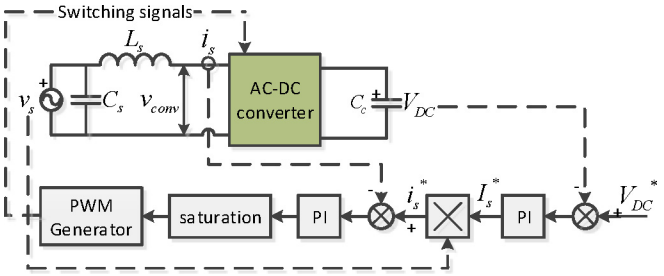

Figure 8. Conventional AC-DC converter control diagram

To get rid of phase distortion, decrease the harmonics pollution, and get faster dynamic response, a Predictive Current Control (PCC) strategy combined with PLL and band-stop filter is designed. The control diagram of PCC with PLL and band-stop filter is shown in Figure 9.

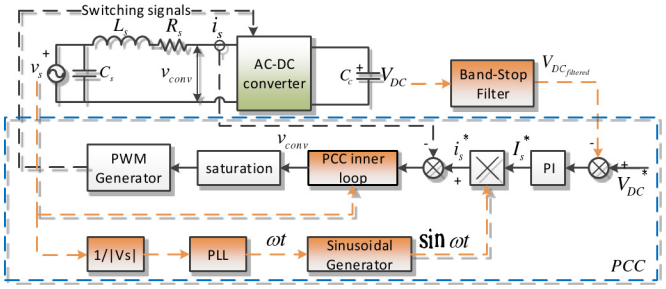

Figure 9. Predictive Current Control diagram

I Figure 7, the input power on grid side is expressed in equation (17).

$$\begin{aligned} Power_{in} &= v_s \cdot i_s = V_s sin\omega t \cdot I_s \sin(\omega t - \theta) \\ &= \mathrm{V_s} I_s sin\omega t \cdot (sin\omega t cos\theta - cos\omega t sin\theta) \end{aligned} \tag{17}$$

Since θ equals to 0° or 180° , $sin\theta = 0$, the input power can be expressed as equation (18) as well.

$$\begin{aligned} Power_{in} &= \mathrm{V_s} I_s \sin^2 \omega t cos\theta \\ &= \mathrm{V_s} I_s \cdot \frac{1 - \cos(2\omega t)}{2} \cdot cos\theta \\ &= \frac{\mathrm{V_s} I_s}{2} cos\theta - \frac{V_s I_s}{2} cos\theta \cos(2\omega t) \end{aligned} \tag{18}$$

where $-\frac{V_s I_s}{2} cos\theta \cos(2\omega t)$ is the distortion part of the input power. According to Figure 6, the output power of the converter is expressed as equation (19).

$$Power_{out} = \mathrm{V_{DC}} \cdot I_L + C_c V_{DC} \frac{d\tilde{v}_{DC}}{dt} \tag{19}$$

where $\tilde{v}_{DC}$ is the second order ripple on DC link voltage, and $C_c V_{DC} \frac{d\tilde{v}_{DC}}{dt}$ is the distortion part on output power. Assume that there is no power loss for switches, we have $Power_{in}$, equals to $Power_{out}$, and distortion part equals to each other.

$$C_c V_{DC} \frac{d\tilde{v}_{DC}}{dt} = -\frac{V_s I_s}{2} cos\theta \cos(2\omega t) \tag{20}$$

Therefore, the ripple on DC link voltage is obtained in equation (21). It is observed that the frequency of the ripple is twice as the grid frequency. If this ripple is introduced in the controller and multiplied with the grid voltage which has the first order frequency, the third order harmonic will be generated, meanwhile, more odd harmonics will be generated.

$$\tilde{v}_{DC} = -\frac{V_s I_s}{4\omega C_c V_{DC}} cos\theta \sin(2\omega t) \tag{21}$$

To decrease the harmonics pollution, a second order band-stop (notch) filter is employed. In SimPowerSystems, this filter implements the following transfer function.

$$H(s) = \frac{s^2 + \omega_n^2}{s^2 + 2\zeta\omega_n s + \omega_n^2} \tag{22}$$

Where s is the Laplace operator; ω_n is the natural frequency that equals to $2\pi f_n$; and ζ is the damping ratio. In this case, f_n is 120Hz, and ζ is 0.707, so that the filter quality Q equals to $\frac{1}{2\zeta}$, which is 0.707, and bandwidth β equals to $\frac{f_n}{Q}$, which is $2\zeta f_n$ Hz.

A 120Hz band-stop filter is added before V_{DC} entering the outer voltage control loop. The filtered V_{DC} and original V_{DC} are compared in Figure 10. It is observed that, the second order harmonic on original DC link voltage is filtered.

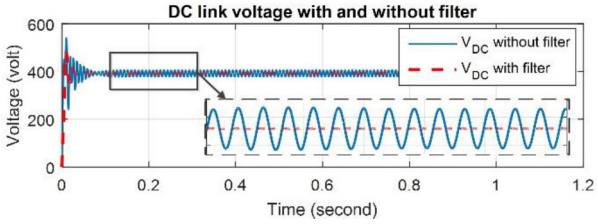

Figure 10. Comparison between original DC voltage and filtered DC voltage

PLL technology is applied to lock the phase information of the undistorted fundamental grid voltage. The phase lock loop control diagram is shown in Figure 11 [34]. The phase detector converts the phase difference between input phase and output phase to a proportional voltage signal with a variable frequency mean value. A proportional-integral-derivative (PID) controller with an automatic gain control makes the phase difference to be zero by acting on a voltage-controlled-oscillator, meanwhile, a mean frequency is obtained by filtering the output of the PID controller [34].

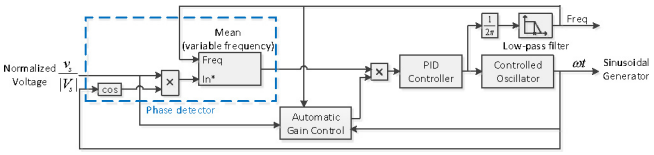

Figure 11. Phase lock loop control diagram [34]

Figure 12 shows the PLL control results. PLL frequency is locked at 60Hz. From the peak difference on x-axis between PLL result and v_s fundamental signal, the phase distortion is fixed, and the unwanted information due to phase distortion is avoided.

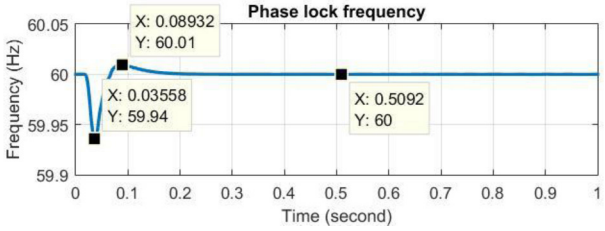

a.

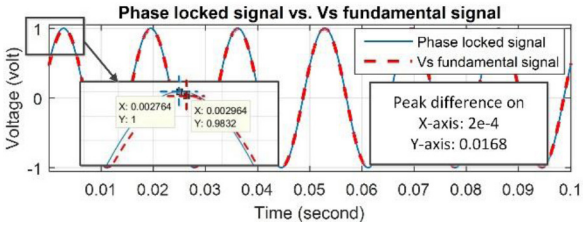

b.

Figure 12. PLL technique application in AC-DC converter. a. Frequency lock process. b. Phase locked signal versus Vs fundamental signal.

PCC is aimed to equal the sensed grid current i_s to the reference grid current i_s^* in one PWM period T_s. The current should meet the following equations:

$$i_s(t_n + T_s) = i_s^*(t_n) \tag{23}$$

$$L_s \frac{di_s}{dt} = L_s \frac{i_s(t_n+T_s) - i_s(t_n)}{T_s} = L_s \frac{i_s^*(t_n) - i_s(t_n)}{T_s} \tag{24}$$

$$v_{conv} = v_s - R_s i_s - \frac{L_s(i_s^* - i_s)}{T_s} \tag{25}$$

Since R_s is very small, the value is ignored, and PCC algorithm is expressed as equation (26). I_s^* is the output of the outer-loop PI controller in Figure 9.

$$\begin{cases} v_{conv}(t) = v_s(t) - \frac{L_S}{T_s}[I_s^* \sin(\omega t) - i_s(t)] \\ I_s^* = K_p(V_{DC}^* - V_{DC}) + K_i \int (V_{DC}^* - V_{DC}) dt \end{cases} \tag{26}$$

Figure 13 shows the detailed PCC inner loop circuit diagram, since R_s is ignored in equation (26), in this diagram, it is presented in dash line.

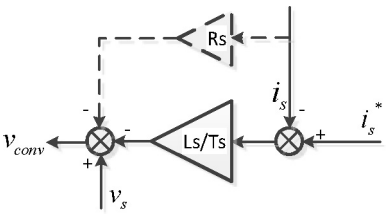

Figure 13. PCC inner loop circuit diagram.

BI-DIRECTIONAL PWM DC-DC CONVERTER

Model Structure of DC-DC Converter

In this paper, a bi-directional half-bridge buck-boost PWM DC-DC converter is used to transmit power between AC-DC converter and battery. This converter consists of two IGBTs with the internal diodes, one inductor, and one capacitor. The Simulink model of the DC-DC converter connected with battery is shown in Figure 14.

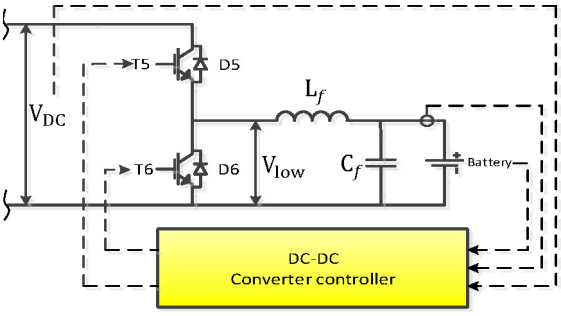

Figure 14. DC-DC converter connected with battery

For the DC-DC converter output LC filter design, the capacitor and inductor are selected based on the cutoff frequency f_c defined in equation (27). The purpose of adding the low pass filter is to filter the undesired harmonics caused by switching frequency, hence, the cutoff frequency is selected to be less than the switching frequency f_s. In this paper, L_f is 100μH, C_f is 100μF, and f_s is 20 kHz.

$$f_c = \frac{1}{2\pi\sqrt{LC}} < f_s \tag{27}$$

The converter is in a buck mode when battery is being charged and a boost mode when battery is discharging. The circuit descriptions are shown in Figure 15 and Figure 16. In charging mode, when T_5 is on and T_6 is off, two diodes are reversely biased; when both T_5 and T_6 are off, D_6 is conducted to release the energy stored in the inductor.

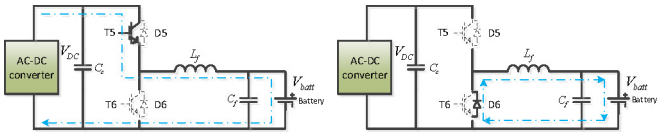

a. b.

Figure 15. DC-DC converter circuit description in buck mode. a. T_5 on, T_6 off; b. T_5 off, T_6 off . The dash arrow represents the current path, for IGBTs, the solid line means on, and dash line means off.

When the converter works as a boost converter, the battery is discharged. When T_6 is turned on and T_5 is off, the current goes in the reverse direction. When both T_5 and T_6 are turned off, D_5 is conducted. The battery feeds the power back to the grid through AC-DC converter.

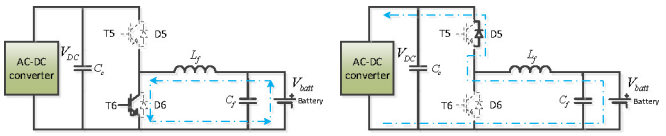

a. b.

Figure 16. DC-DC converter circuit description in boost mode. a. T_6 on, T_6 off; b. T_5 off, T_6 off. The dash arrow represents the current path, for IGBTs, the solid line means on, and dash line means off.

The switching signal of buck and boost mode are defined as g_{buck} and g_{boost}, respectively. The buck and boost mode is controlled by PWM switching signals generated by constant voltage (CV) and constant current (CC) control methods. In this paper, CV-CC dual PI control is applied in battery charging mode. CC control method is applied in discharging mode shown in Figure 18. As shown in Figure 17 shows the control strategy for battery charging. The outer voltage control loop generates a battery current reference for the inner current control, and then provide a controlled voltage for PWM signal generation.

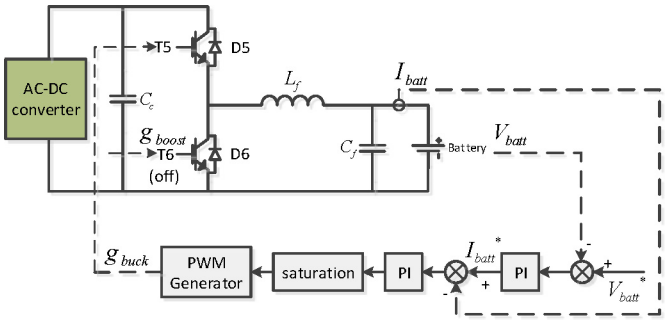

Figure 17. Constant Voltage and Constant Current control in charging mode

For battery discharging, the constant current control algorithm is shown in equations (28) [35] and (29) [35]. The control diagram is shown in Figure 18.

$$g_{boost_{steady}} = 1 - \frac{V_{batt}}{V_{DC}} \tag{28}$$

$$g_{boost} = g_{boost_{steady}} + (K_p + \frac{K_I}{S}) \times (I^*_{batt} - I_{batt}) \tag{29}$$

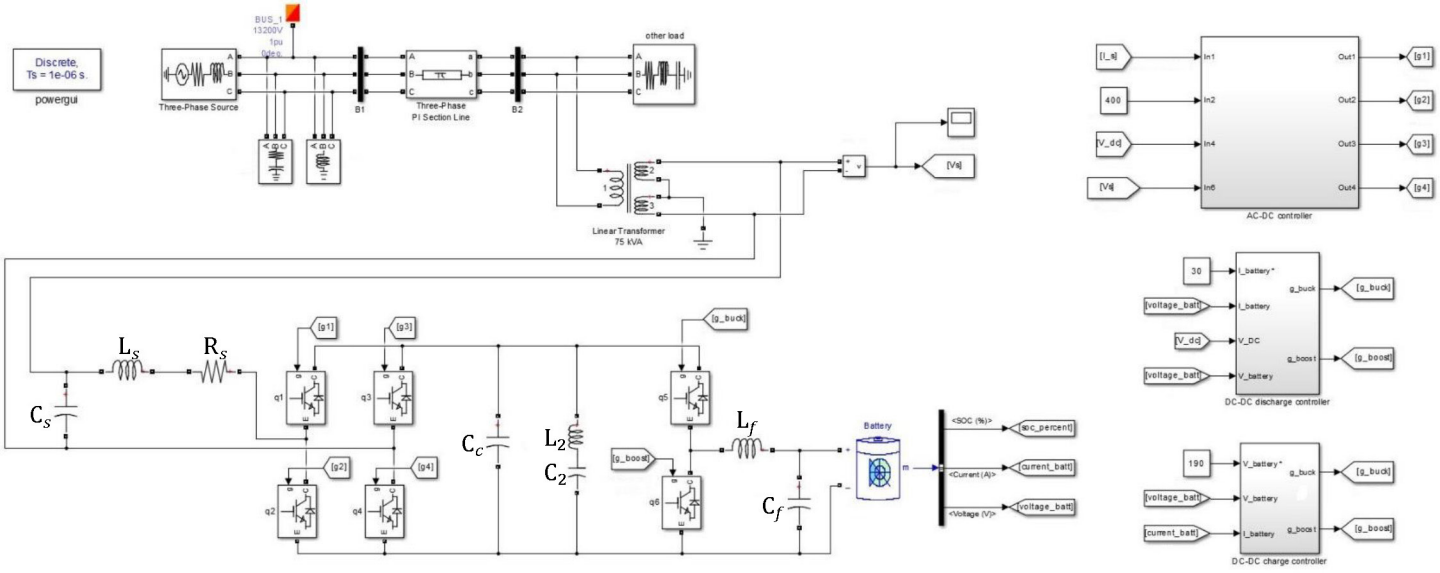

Figure 19. Bi-directional PEV charging system model in Simulink/SimPowerSystems

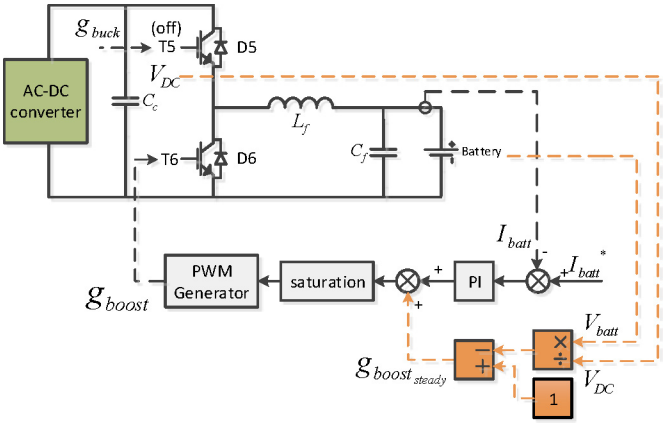

Figure 18. Constant Current control in discharging mode

SIMULATION RESULTS AND ANALYSIS

The Simulink model of the charging system is shown in Figure 19. The model parameters are tabulated in Table 3.

Table 3. Model Parameters

Parameters	Values
V_{s-rms} (grid voltage)	$240Vrms$
f (grid fundamental frequency)	$60Hz$
L_s (inductance on grid side)	$2mH$
R_s (resistance on grid side)	0.003Ω
C_c (conductance on DC link)	$8mF$
L_2 (inductance of DC link filter)	$0.84mH$
C_2 (conductance of DC link filter)	$3mF$
L_f (inductance on battery side)	$100\mu H$
C_f (conductance on battery side)	$100\mu F$
V_{DC}^* (DC link reference voltage)	$400V$
f_s (switching frequency for DC-DC converter and AC-DC converter)	$20kHz$

The simulation results are shown to test the following three aspects: Having Unity Power factor, Total Harmonics Distortion analysis, Capability of Bi-directional Power Flow.

Realization of Unity Power Factor

AC power has active power P, and reactive power Q, their vector sum is S, where $S^2 = P^2 + Q^2$, and the cosine of the phase angle between P and S is defined as power factor $\frac{|P|}{|S|}$. Unity power factor can be obtained when the current and voltage have the same phase or in a circuit where only contains resistive load. In this study, the non-linear load, such as rectifier, that causes current harmonic distortion, may reduce power factor. In addition, the phase shifting of grid voltage is one factor causes power factor reduction. PLL and Band-stop filter, therefore, contribute to the unity power factor. In Figure 20, the grid voltage and grid current has the same phase in charging mode, and a phase difference of 180 degrees in discharging mode, so, the unity power factor is achieved in this study.

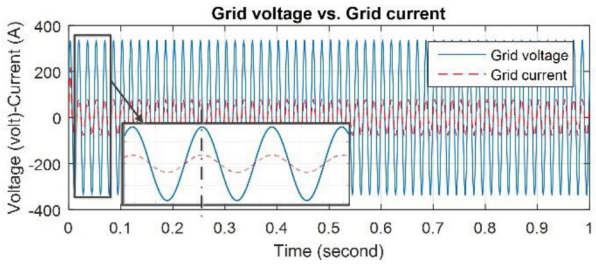

a.

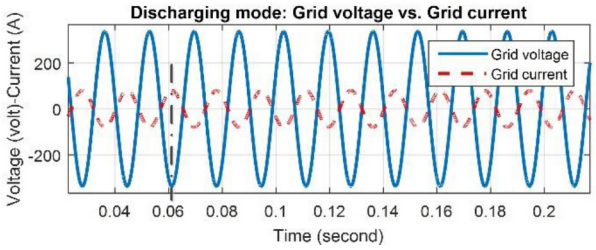

b.

Figure 20. Waveforms of Grid voltage and Grid current. a. Charging mode; b. Discharging mode.

Total Harmonics Distortion Analysis

In utility distribution system, the harmonics distortion is typically caused by nonlinear load. Harmonics are characterized by distortion factor (DF) that is defined as the ratio of the root-mean-square of the harmonic content to the root-mean-square value of the fundamental quantity [28]. Total Harmonic Distortion (THD) is commonly used to define either voltage or current DF. For current, THD is defined in equation (30).

$$\mathrm{THD}_I = \frac{\sqrt{\sum_{n=2}^{\infty} I_{n_{rms}}^2}}{I_{1_{rms}}} \cdot 100\% \tag{30}$$

where n is the order of harmonics, $I_{n_{rms}}$ is the root-mean-square value of the n^{th} order harmonics for current. Figure 21 shows the FFT (Fast Fourier Transform) analysis of the grid current. The grid current THD value is 1.99%, that meets the IEEE Std 519 [28] requirement of current THD, less than 5.0%. Comparing with the results from conventional controlled method, the THD of the presented control method is 3.81% less.

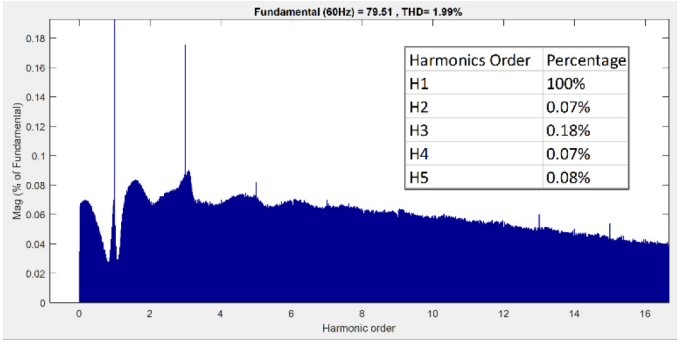

a.

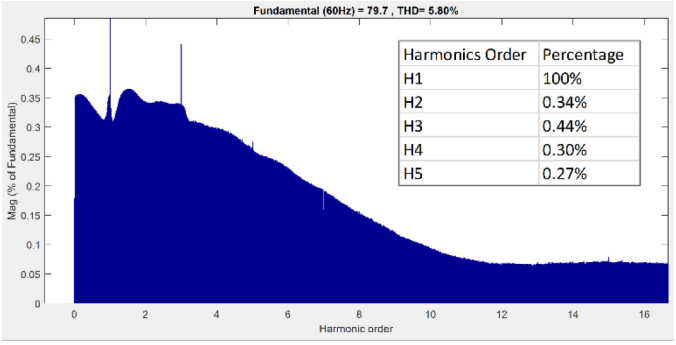

b.

Figure 21. FFT analysis for grid current. a. PCC strategy; b. Conventional strategy

Capability of Bi-Directional Power Flow

In this simulation, the initial SOC is set as 50%. It is observed from Figure 22 that the DC link voltage is 400V±2% in both charging and discharging mode. In Figure 23, the battery is charging at constant voltage 196V and constant current -67A. From these results, it is concluded that the system has good performance in relative high power condition. In Figure 24, the battery is controlled to discharge at constant current 30A, and the discharging voltage is 194V. This indicates the CC-CV charging control and CC discharging control can realize the bi-directional power flow.

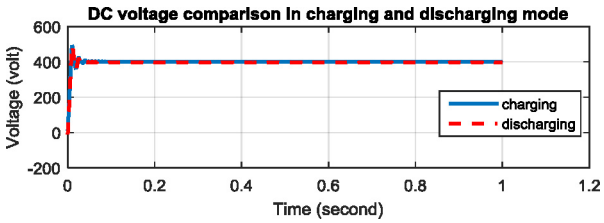

Figure 22. DC link voltage in charging and discharging mode

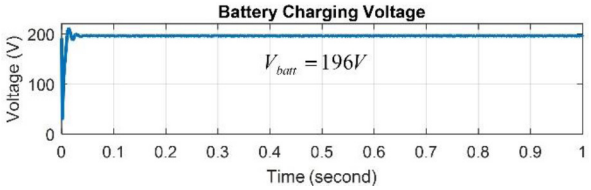

a.

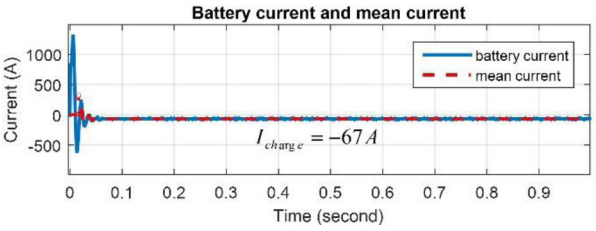

b.

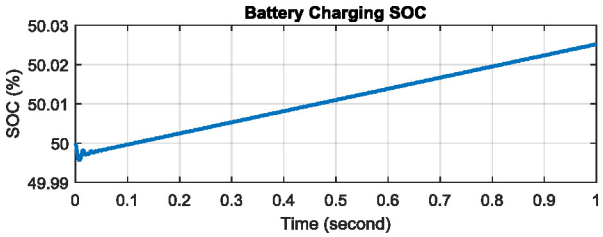

c.

Figure 23. Battery performance in charging mode. a. Battery voltage; b. Battery current; c. Battery SOC.

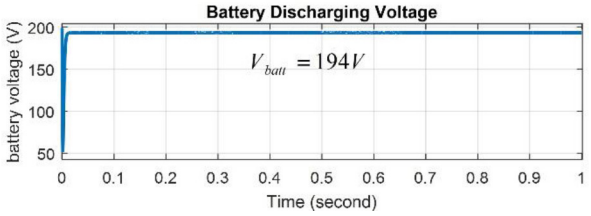

a.

Figure 24. Battery performance in discharging mode. a. Battery voltage; b. Battery current; c. Battery SOC.

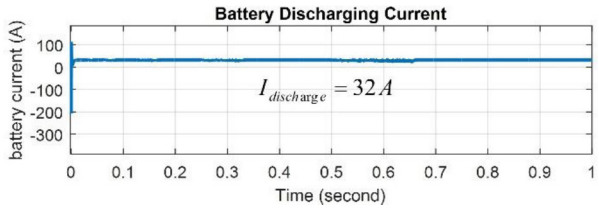

b.

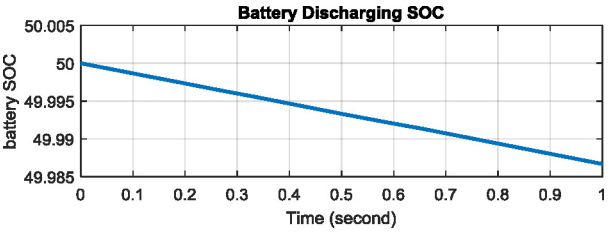

c.

Figure 24 (cont). Battery performance in discharging mode. a. Battery voltage; b. Battery current; c. Battery SOC.

SUMMARY/CONCLUSIONS

In this paper, a grid-tied single phase bi-directional PEVs charging system is developed using SimPowerSystems in Matlab/Simulink environment. The structures of the AC-DC converter and DC-DC converter are presented, respectively. To achieve good current regulation and constant DC-link voltage, Predictive Current Control strategy is applied. In addition, the PLL technology and band-stop filter are designed in the model to avoid the introduction of odd harmonics and distorted grid phase information into the controller.

A simulation test has been conducted. The results show that the presented charging system has the capability of bi-directional power flow and can achieve unity power factor. Predictive Current Control strategy combined with PLL and band-stop filter improves the performance of the charging system that phase shifting of grid voltage is avoided and second order harmonics on DC link voltage is filtered. THD of grid current is decreased by 3.81% comparing with conventional control method. In summary, this charging system effectively performs the role of interface between the grid and PEVs.

Future work is recommended as following: (1). Expand AC charging to DC fast charging; (2). Consider the PEV charging problem for a fleet of vehicles instead of one vehicle; (3). Study the impact of the PEV charging on grid with various PEV penetration rate; (4). Study the effect of reverse power service on battery lifetime; (5). Integrate PEVs with renewable energy sources, such as solar panels, and control the charging/discharging behavior of PEVs to effectively balance the grid load demand at an acceptable level.

REFERENCES

1. EPA and NHTSA, 2017 and Later Model Year Light-Duty Vehicle Greenhouse Gas Emissions and Corporate Average Fuel Economy Standards; Final Rule, F. Register, 2012. Available from: https://www.federalregister.gov.
2. DOE, "vehicle technologies". Available from: http://energy.gov/eere/vehicles/vehicle-technologies-office-batteries/.
3. Hyosung K., Taesik Y., and Sewan C., "Indirect Current Control Algorithm for Utility Interactive Inverters in Distributed Generation Systems," Power Electronics, IEEE Transactions on, vol. 23, pp. 1342-1347, 2008.
4. Sriram V. B., SenGupta S., and Patra A., "Indirect current control of a single-phase voltage-sourced boost-type bridge converter operated in the rectifier mode," Power Electronics, IEEE Transactions on, vol. 18, pp. 1130-1137, 2003.
5. Malesani L. and Tomasin P., "PWM current control techniques of voltage source converters-a survey," in Industrial Electronics, Control, and Instrumentation, 1993. Proceedings of the IECON '93., International Conference on, 1993, pp. 670-675 vol.2.
6. Brod D. M. and Novotny D. W., "Current Control of VSI-PWM Inverters," Industry Applications, IEEE Transactions on, vol. IA-21, pp. 562-570, 1985.
7. Srikanthan S. and Mishra M. K., "Constant frequency current control using a ramp comparison method for a DSTATCOM application," in TENCON 2008 - 2008 IEEE Region 10 Conference, 2008, pp. 1-6.
8. Daniyal H., Lam E., Borle L. J., and Iu H. H. C., "Hysteresis, PI and Ramptime Current Control Techniques for APF: An experimental comparison," in Industrial Electronics and Applications (ICIEA), 2011 6th IEEE Conference on, 2011, pp. 2151-2156.
9. Bin Y. and Liuchen C., "Improved Predictive Current Controlled PWM for Single-Phase Grid-Connected Voltage Source Inverters," in Power Electronics Specialists Conference, 2005. PESC '05. IEEE 36th, 2005, pp. 231-236.
10. Kojabadi H. M., Bin Y., Gadoura I. A., Liuchen C., and Ghribi M., "A novel DSP-based current-controlled PWM strategy for single phase grid connected inverters," Power Electronics, IEEE Transactions on, vol. 21, pp. 985-993, 2006.
11. Holmes D. G. and Martin D. A., "Implementation of a direct digital predictive current controller for single and three phase voltage source inverters," in Industry Applications Conference, 1996. Thirty-First IAS Annual Meeting, IAS '96., Conference Record of the 1996 IEEE, 1996, pp. 906-913 vol.2.
12. Yong X., Yuchuan W., and Haixia Z., "An Adaptive Predictive Current-Controlled PWM Strategy for Single-Phase Grid-Connected Inverters," in Industrial Electronics Society, 2007. IECON 2007. 33rd Annual Conference of the IEEE, 2007, pp. 1548-1552.
13. Zhang X., Xuhui W., Zhao F., and Guo X., "A new control strategy for bi-directional DC-DC converter in electric vehicle," in Electrical Machines and Systems (ICEMS), 2011 International Conference on, 2011, pp. 1-4.
14. Premananda Pany R. K. S., Tripathi R.K, "Bidirectional DC-DC converter fed drive for electric vehicle system," International Journal of Engineering, Science and Technology, vol. 3, pp. 101-110, 2011.
15. Young-Joo L., Khaligh A., and Emadi A., "Advanced Integrated Bidirectional AC/DC and DC/DC Converter for Plug-In Hybrid Electric Vehicles," Vehicular Technology, IEEE Transactions on, vol. 58, pp. 3970-3980, 2009.
16. Dubey A., Santoso S., and Cloud M. P., "Average-value model for plug-in hybrid electric vehicle battery chargers," in Power and Energy Society General Meeting, 2012 IEEE, 2012, pp. 1-8.
17. Leeb S. B., Mitwalli A. H., Jackson D. K., and Verghese G. C., "A multirate digital controller for an electric vehicle battery charger," in Power Electronics Specialists Conference, 1996. PESC '96 Record., 27th Annual IEEE, 1996, pp. 1919-1925 vol.2.
18. Cong-Long N. and Hong-Hee L., "AC voltage sensorless control of battery charger system in electric vehicle applications," in IPEC, 2012 Conference on Power & Energy, 2012, pp. 515-520.
19. C.-L. Nguyen and Lee H.-H., "An effective control scheme for a universal input battery charger in electric vehicle applications," in Strategic Technology (IFOST), 2012 7th International Forum on, 2012, pp. 1-6.
20. Bilgin, E. Dal Santo B., and Krishnamurthy M., "Universal input battery charger circuit for PHEV applications with simplified controller," in Applied Power Electronics Conference and Exposition (APEC), 2011 Twenty-Sixth Annual IEEE, 2011, pp. 815-820.
21. Ebrahimi S., Tagliavi M., Tahami F. , and Oraee H., "A single-phase integrated bidirectional plug-in hybrid electric vehicle battery charger," in Industrial Electronics Society, IECON 2014 -40th Annual Conference of the IEEE, 2014, pp. 1137-1142.
22. Xiaohu Z., Lukic S., Bhattacharya S., and Huang A., "Design and control of grid-connected converter in bi-directional battery charger for Plug-in hybrid electric vehicle application," in Vehicle Power and Propulsion Conference, 2009. VPPC '09. IEEE, 2009, pp. 1716-1721.

23. Ota Y., Taniguchi H., Suzuki H., Nakajima T., Baba J., and Yokoyama A., "Implementation of grid-friendly charging scheme to electric vehicle off-board charger for V2G," in Innovative Smart Grid Technologies (ISGT Europe), 2012 3rd IEEE PES International Conference and Exhibition on, 2012, pp. 1-6.
24. Arancibia A. and Strunz K., "Modeling of an electric vehicle charging station for fast DC charging," in Electric Vehicle Conference (IEVC), 2012 IEEE International, 2012, pp. 1-6.
25. Kang T. Miao, V. Ramachandaramurthy K., and Jia Ying Y., "Bidirectional battery charger for electric vehicle," in Innovative Smart Grid Technologies - Asia (ISGT Asia), 2014 IEEE, 2014, pp. 406-411.
26. Verma A. K., Singh B., and Shahani D. T., "Grid to vehicle and vehicle to grid energy transfer using single-phase bidirectional AC-DC converter and bidirectional DC-DC converter," in Energy, Automation, and Signal (ICEAS), 2011 International Conference on, 2011, pp. 1-5.
27. Monteiro V., Exposto B., Pinto, J. G. Almeida R., Ferreira J. C., Nogueiras Melendez A. A., et al., "On-board electric vehicle battery charger with enhanced V2H operation mode," in industrial Electronics Society, IECON 2014 - 40th Annual Conference of the IEEE, 2014, pp. 1636-1642.
28. "IEEE Recommended Practices and Requirements for Harmonic Control in Electrical Power Systems," IEEE Std 519-1992, pp. 1-112, 1993.
29. EIA, "Annual Energy Review 2011" Available from: http://www.eia.gov/aer/.
30. Hybrid Auto Center LLC, “60Ah Nissan Leaf Battery Module,” Available from: http://www.hybridautocenter.com/.
31. He H., Xiong R., and Fan J., "Evaluation of Lithium-Ion Battery Equivalent Circuit Models for State of Charge Estimation by an Experimental Approach," Energies, vol. 4, p. 582, 2011.
32. Matlab/Simulation-SimPowerSystems-Battery, available from: http://www.mathworks.com/.
33. SAE International Surface Vehicle Recommended Practice, "SAE Electric Vehicle and Plug in Hybrid Electric Vehicle Conductive Charge Coupler," SAE International Standard J17722, Rev. Jan. 2010.
34. Matlab/Simulation-SimPowerSystems-PLL, available from: http://www.mathworks.com/.
35. Arancibia A. and Strunz K., "Modeling of an electric vehicle charging station for fast DC charging," in Electric Vehicle Conference (IEVC), 2012 IEEE International, 2012, pp. 1-6.